Nigerian Research Journal of Chemical Sciences (ISSN: 2682-6054)
Volume 13, Issue 2, 2025

Synthesis and Luminescent Properties of Transition Metal Coordination Polymers of Multidentate Carboxylate and N-Donor Ligands

*[1]Victoria T. Olayemi, [1]Ayobami C. David, [1]Bolatito E. Olanipekun, [1]Damilola T. Ogundele, [1]John O. Abedoh and [1,2]Basheer A. Jaji

[1]Department of Chemistry and Industrial Chemistry, Faculty of Pure and Applied Sciences, Kwara State University, Malete, Nigeria.

[2]Department of Physical & Chemical Sciences, Faculty of Sciences, Federal University of Health Sciences, Ila-Orangun, Nigeria.

*Corresponding Author: tosin.bodunde@kwasu.edu.ng

Accepted: September 26, 2025. Published Online: September 28, 2025

ABSTRACT

In this study, four transition metal coordination polymers were synthesized $[Zn(BDC)_2(TMP)_2(H_2O)_2]_n$, $[Cu(BDC)_2(TMP)_2(H_2O)_2]_n$, $[Zn(PDC)_2(BTEC)_2(H_2O)_2]_n$, and $[Cu(PDC)_2(BTEC)_2(H_2O)_2]_n$, where BDC = 1,4-benzenedicarboxylic acid, TMP = 4,4′-trimethylenedipyridine, PDC = 2,6-pyridinedicarboxylic acid, and BTEC = 1,2,4,5-benzenetetracarboxylic acid. The coordination polymers were synthesized via a solvothermal method in a Teflon-lined autoclave. The products were characterized by Fourier-transform infrared spectroscopy (FTIR), UV–Vis spectroscopy, Thermogravimetric analysis (TGA), Scanning electron microscopy (SEM), and Brunauer–Emmett–Teller (BET) surface area analysis. Furthermore, their luminescent properties were examined by photoluminescent spectroscopy (PLS). FTIR spectra shows characteristic bands of ν(C=O), ν(M-O) and ν(M-N) confirming successful coordination of the carboxylate/nitrogen donor ligands to the transition metal centers. UV–Vis spectroscopy revealed intra-ligand $\pi \rightarrow \pi^*$ and $n \rightarrow \pi^*$ transitions, ligand-to-metal charge transfer (LMCT) bands, and d–d transitions in the Cu-based frameworks. Photoluminescence studies showed that the metal organic frameworks (MOFs) exhibited strong ligand-centred emissions, which were blue-shifted compared with the free ligands due to metal–ligand coordination.

Keywords: Coordination polymers, photoluminescence, solvothermal synthesis, ligand-to-metal charge transfer and transition metal complexes.

INTRODUCTION

Coordination polymers (CPs) are a class of crystalline material possessing nanopore network structure, which are formed by self-assembly of coordination between transition-metal cations and oxygen or nitrogen containing polydentate organic linkers [1]. It is a new class of porous coordination polymers composed of organic ligands and metal nodes, having characteristic features such as porous structure with tuneable pore size, large surface area, good thermal stability, superior catalytic activity, wide variation in secondary building unit (SBU), abundant functional groups, exclusive optical properties, and enormous absorption capacity. The ligand functions as an electron donor via its lone pair, and its structural characteristics significantly influence the resulting pore size of the framework. The metal component on the other hand, determine the dimensionality of the MOF [2]. It may vary from the s-block, p-block, transition metals, or even rare earth metals.

Transition metals are characterized with desirable properties such as variable oxidation states, coordination versatility, partially filled d-orbitals, strong metal–ligand bonding, lewis acidity, magnetic moment, and ability to activate substrates. These characteristics have been crucial in fabricating coordination polymers (CPs), enabling their diverse applications in magnetism [3], gas adsorption [4], luminescence [5], Chemical Sensing [6] and catalysis [7]

In recent years, fluorescence-based detection has emerged as focal point in optical sensing research, owing to its advantages of user-friendliness, compact design, fast analysis time, affordability, high sensitivity and selectivity [8]. MOFs are highly suitable for fabricating luminescent materials because they possess attractive characteristics such as Straightforward synthesis, predictable structures, nanoscale processability, collaborative multifunctionalities [9]. Traditional porous solids often exhibit limited framework diversity, modest chemical functionality and lack intrinsic, tunable luminescence. In contrast, MOFs offer modular design of both metal nodes and organic linkers, enabling precise control over pore size, surface area and emission behavior within a single crystalline platform. This allows for high selectivity through pore-sieving or host-guest interactions [10].

This study aims to synthesize Cu(II) and Zn(II) metal organic frameworks based on multidentate and N-donor ligands and investigate their luminescent properties for potential use in chemical sensing. The specific objectives of this study are to prepare metal organic frameworks

via solvothermal method and characterize the synthesized MOFs using FTIR, UV–Vis spectroscopy, PLS, TGA, SEM, and BET surface area analysis.

MATERIALS AND METHODS

Materials

All reagents and chemicals were of analytical grade and were used as received without further purification. All the ligands used; 1,4-benedicarboxylic acid, 4,4-trimethylenedipyridine, 2,3-pyridinedicaboxylic acid, and 1,2,4,5-benzenetetracarboxylic acid were purchased from Sigma Aldrich, Germany. The metal salts, Zinc nitrate hexahydrate ($Zn(NO_3)_2.\ 6H_2O$) and Copper nitrate trihydrate ($Cu(NO_3)_2.\ 3H_2O$) along with other reagents like ethanol (98.8%), *N,N*-dimethyl formamide (DMF) (99.0%) were obtained from commercial chemical stores in Nigeria.

Instrumentation

The infrared spectra were recorded using a Shimadzu FTIR-8400S spectrometer using KBr plate method. UV-Vis absorption spectra were measured in the range 200 to 800 nm using an Agilent Cary Spectrophotometer with a slit width of 2 nm. The fluorescence emission spectra were recorded on an Agilent Cary Eclipse Photoluminescence Spectrometer set at 2.5 nm slit width for both the excitation and emission. TGA was performed using an SDT-Q600 TA instrument. The sample was heated in air with a heating rate of 10 ºC min^{-1} and the scan was recorded within the temperature range of 25-900 °C. Scanning Electron Microscopy was conducted on a JOEL-JSM 7600 F microscope at 20 KV.

Synthesis of the CPS

The MOFs were synthesized via a solvothermal method in a Teflon-lined autoclave, following literature precedents [9,11] with slight stoichiometric modifications.

Synthesis of $[Zn(BDC)_2(TMP)_2].2H_2O$ (1)

$Zn(NO_3)_2{\cdot}6H_2O$ (2 mmol, 0.594 g), 4,4′-trimethylenedipyridine (TMP) (1 mmol, 0.198 g), and 1,4-benzenedicarboxylic acid (BDC) (2 mmol, 0.332 g) were each dissolved in 5 mL DMF. The three solutions were mixed to form a homogeneous reaction mixture and transferred to a Teflon-lined autoclave. The reaction was carried out at 120 °C for 24 h, then cooled to room temperature

(Scheme 1). The resulting solid was filtered, washed with DMF, and dried at room temperature for 12 h. The complex, **1** was obtained as orange-red granulated crystals (0.70 g, ≈62.3 % yield).

Synthesis of $[Cu(BDC)_2(TMP)_2].2H_2O$ (2)

Following the same protocol as in CP **1**, $Cu(NO_3)_2 \cdot 3H_2O$ (2 mmol, 0.484 g) replaced the zinc salt, with TMP (1 mmol, 0.198 g) and BDC (2 mmol, 0.332 g). After solvothermal treatment, **2** was isolated as a fine blue powder (0.50 g, ≈49.3 % yield).

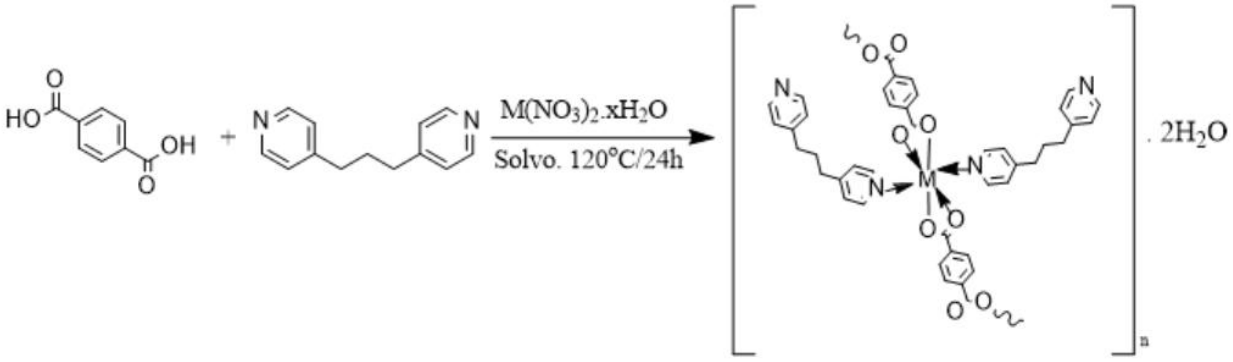

Scheme 1: Reaction pathway for the synthesis of CP **1** and CP **2**

Synthesis of $[Zn(PDC)_2(BTEC)_2]_n.2H_2O$ (3)

$Zn(NO_3)_2 \cdot 6H_2O$ (2 mmol, 0.594 g), 2,6-pyridinedicarboxylic acid (PDC) (1 mmol, 0.167 g), and 1,2,4,5-benzenetetracarboxylic acid (BTEC) (2 mmol, 0.508 g) were each dissolved in 5 mL of DMF. The mixture was reacted under identical solvothermal conditions (Scheme 2). The resulting bright white powder **3**, (0.60 g, ≈47.3 % yield) was obtained after filtration, washing, and drying.

Synthesis of $[Cu(PDC)_2(BTEC)_2]_n.2H_2O$ (4)

The same procedure was applied as in CP **3**, replacing Zn salt with $Cu(NO_3)_2 \cdot 3H_2O$ (2 mmol, 0.484 g). The product formed, **4** was isolated as a blue powder with block-like aggregation (0.55 g, ≈47.5 % yield).

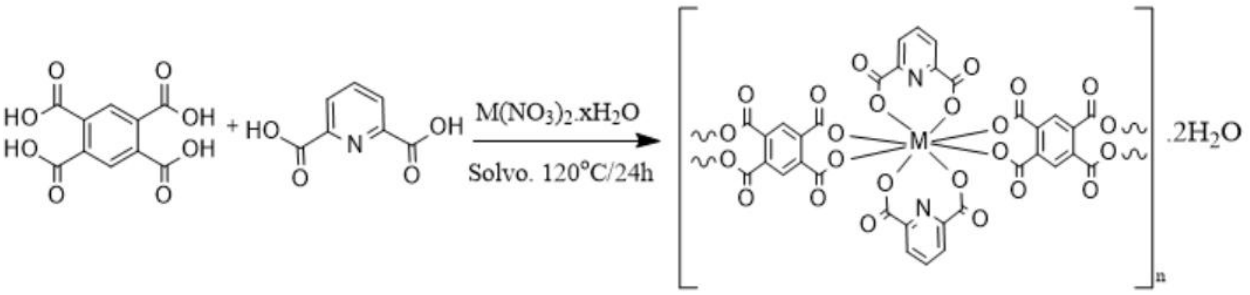

Scheme 2: Reaction pathway for the synthesis of CP **3** and CP **4**

Table 1 gives a summary of reaction conditions, appearance and percentage yield of the synthesized metal organic frameworks.

Table 1. Synthesis conditions, Appearance and Yield

Sample	Metal Salt	Ligands	Temp (°C) / Time	Appearance	Yield
CP 1	$Zn(NO_3)_2 \cdot 6H_2O$	BDC, TMP	120 / 24 h	Orange-red granulated crystals	62.3 %
CP 2	$Cu(NO_3)_2 \cdot 3H_2O$	BDC, TMP	120 / 24 h	Blue powder	49.3 %
CP 3	$Zn(NO_3)_2 \cdot 6H_2O$	PDC, BTEC	120 / 24 h	Bright white powder	47.3 %
CP 4	$Cu(NO_3)_2 \cdot 3H_2O$	PDC, BTEC	120 / 24 h	Blue powder (block-like)	47.5 %

RESULTS AND DISCUSSION

FTIR analysis

The FTIR spectra of the synthesized MOFs and their free ligands are presented in Figure 1. In compound **1** (Figure 1a), a broad absorption around 3465 cm^{-1} corresponds to –OH stretching [12] of terephthalic acid, while peaks at 2949 and 2864 cm^{-1} indicate sp^3 C–H stretching [13] from the TMP ligand. The shift of the sharp C=O band (1740–1700 cm^{-1}) of the free ligand suggests coordination of the carboxylates to the metal center [14]. Aromatic C=C vibrations

appear at 1502–1441 cm^{-1}, and the bands at 577 and 522 cm^{-1} correspond to Zn–O and Zn–N stretching [15], confirming metal–ligand coordination.

For Compound **2** (Figure 1b), a broad –OH band is observed at 3445 cm^{-1} assigned to OH of water, while N–H stretching bands appear at 3081 and 3054 cm^{-1} [13]. The strong absorptions at 1638–1651 cm^{-1} reflect coordinated C=O groups, and an aromatic C=C stretch at 1504 cm^{-1} further supports retention of aromatic moieties. The stretching vibrations of the C=C group is seen at 1385 cm^{-1}, 1226 cm^{-1}, 1106 cm^{-1} and lastly, Cu-O and Cu-N groups are indicated by bands such as 575 cm^{-1}, 505 cm^{-1}, 674 cm^{-1} [12].

Compound **3** (Figure 1c) exhibits a broad –OH band at 3437 cm^{-1}, along with weak sp^3 C–H stretching near 2773 cm^{-1}. The strong bands at 1774 and 1558 cm^{-1} are assigned to C=O/C=C and aromatic C=C vibrations (the aromatic C=C ring in the BTEC ligand is retained), respectively. Intense absorptions in the 1180–1091 cm^{-1} range correspond to C–O groups, while Zn–O and Zn–N stretching is evident at 694 and 420 cm^{-1}.

In compound **4** (Figure 1d), the –OH stretching is shifted to 3475 cm^{-1}, with additional N–H and sp^3 C–H vibrations detected at 3016 and 2935–2817 cm^{-1}. A strong C=O band appears at 1631 cm^{-1}, alongside an aromatic C=C stretch at 1508 cm^{-1}. Multiple C–O stretching bands (1392–1087 cm^{-1}) are retained, and coordination of Cu is confirmed by Cu–O and Cu–N vibrations at 567 and 459 cm^{-1}.

Overall, the disappearance or shift of free ligand carbonyl peaks, coupled with the appearance of M–O/M–N bands in the low-frequency region, strongly supports the successful formation of Zn(II)- and Cu(II)-based CPs.

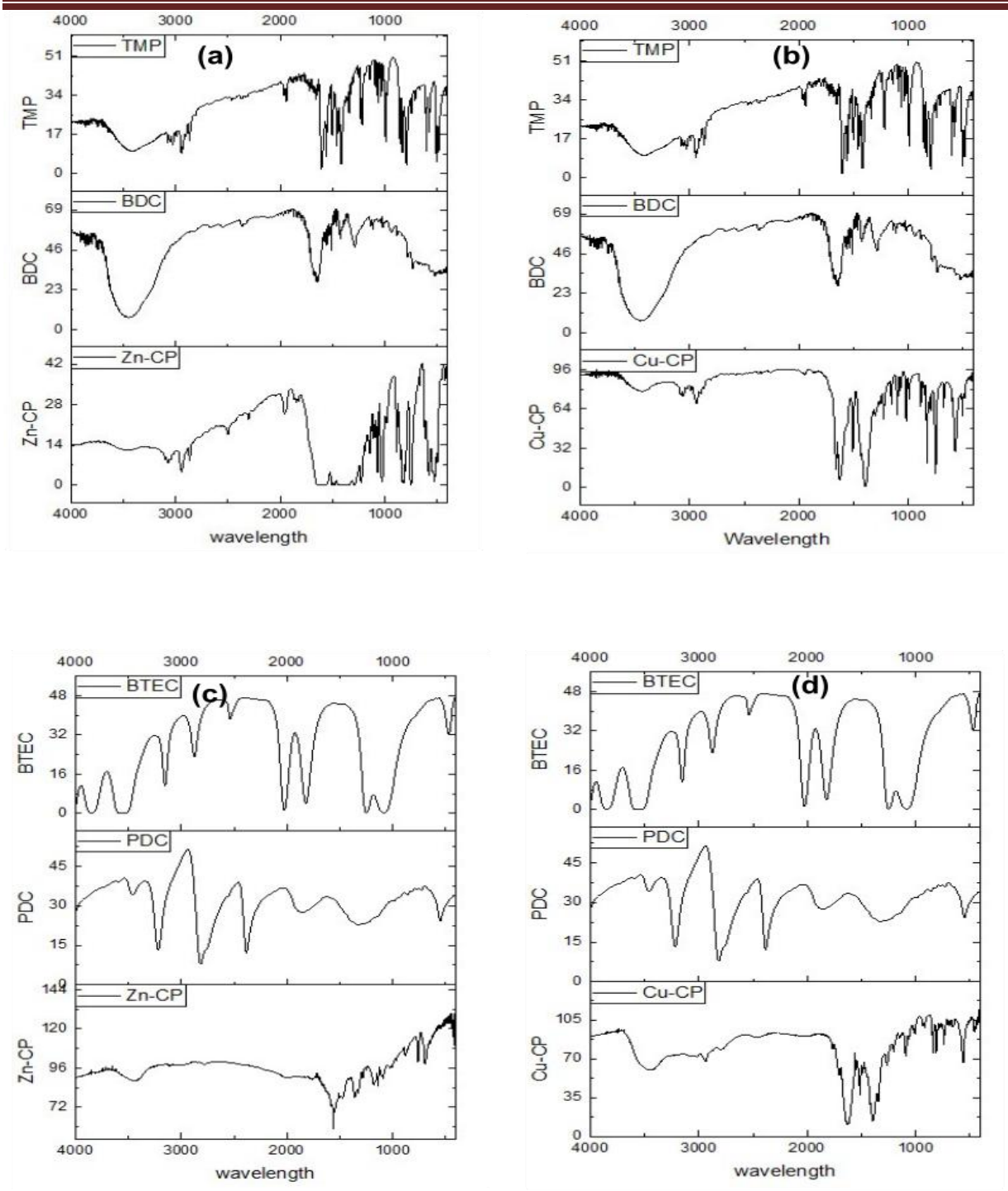

Figure 1. FTIR spectra of the CPs and their ligands: (a) $[Zn(BDC)_2(TMP)_2].2H_2O$ (**1**), (b) $[Cu(BDC)_2(TMP)_2].2H_2O$ (**2**), (c) $[Zn(PDC)_2(BTEC)_2]_n.2H_2O$ (**3**), and (d) $[Cu(PDC)_2(BTEC)_2]_n.2H_2O$ (**4**)

UV/VIS Spectroscopy

The UV/Vis absorption spectra of the ligands and their corresponding CPs are shown in Figure 2. For **1** (Figure 2a), the ligands BDC and TMP display absorption maxima at 274 –295 nm, attributed to π→π* and n→π* transitions. In the band of **1**, these bands are red-shifted to 350–370 nm assigned to ligand-to-metal charge transfer (LMCT) consistent with extended conjugation within the framework. A broad absorption tail at 670 nm is assigned to d-d transition confirms coordination to Zn(II) [16].

The spectrum of compound **2** (Figure 2b) also shows intra-ligand π→π* transitions from BDC (281, 295 nm) and TMP (274 nm). Upon complexation, the CP displays a strong band at 250 nm due to π→π*/ n→π*, inter-ligand charge transfer, along with a red-shifted LMCT band at 372 nm. A broad absorption at 732 nm corresponds to Cu(II) d-d transitions, characteristic of its coordination environment.

For compound **3** (Figure 2c), the free ligands PDC and BTEC show absorptions at 292–310 nm. In the spectrum of **3**, these transitions are shifted to 330 nm, a bathochromic shift indicative of ligand-to-metal charge transfer (LMCT) [17].

Similarly, in compound **4** (Figure 2d), the ligands exhibit absorptions in the 292–310 nm range, whereas the Cu-based MOF displays red-shifted LMCT bands near 370 nm. Additional broad absorptions at 707 and 770 nm are assigned to d–d transitions of Cu(II), confirming its electronic contribution within the framework.

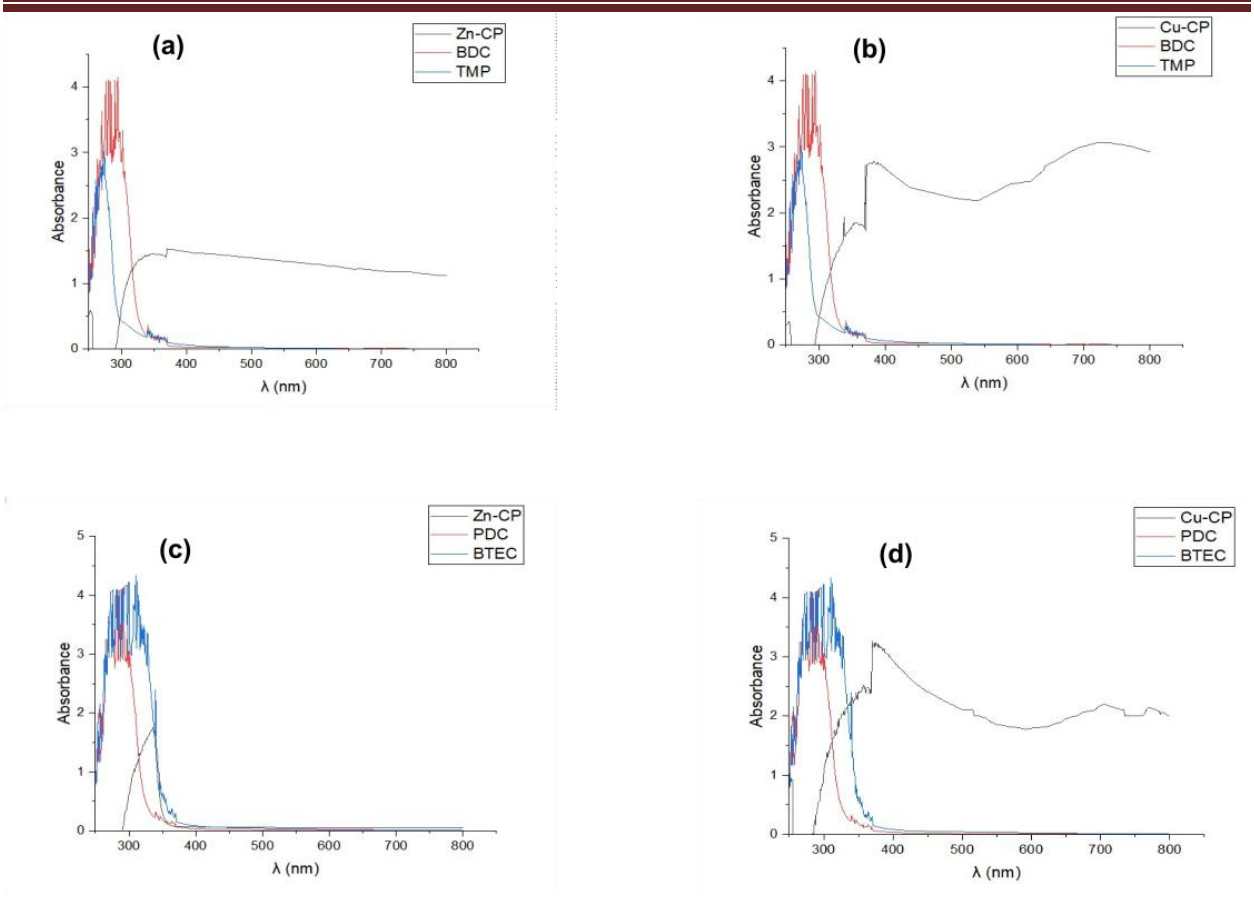

Figure 2. UV/Vis spectra of the ligands and synthesized CPs: (a) $[Zn(BDC)_2(TMP)_2].2H_2O$ (**1**), (b) $[Cu(BDC)_2(TMP)_2].2H_2O$ (**2**), (c) $[Zn(PDC)_2(BTEC)_2]_n.2H_2O$ (**3**), and (d) $[Cu(PDC)_2(BTEC)_2]_n.2H_2O$ (**4**)

Thermal analysis

The TGA profiles of the Zn-based frameworks (**1**, **3**) and Cu-based frameworks (**2**, **4**) revealed the expected multi-step decomposition patterns typical of metal–organic frameworks (Figure 3). All samples showed an initial weight loss below 250 °C, corresponding to removal of lattice or coordinated water (**1**: found 5.38%, calc. 4.35%; **2**: found 3.3%, calc. 4.37%; **3**: found 3.58%, calc. 3.8%; 4: found 3.22%, calc. 3.8%). Framework degradation dominated at higher temperatures. **1** decomposed sharply at ~458 °C with a weight loss of 74.8% (calc. 87.7%), leaving a ZnO residue of 12.23% (calc. 10%). **3** exhibited a major loss of 70.56% up to 509 °C, but retained a larger residue (found 22.49%, calc. 9%), indicating substantial char formation or partial oxidation resistance of Zn species.

The Cu-based samples displayed broader decomposition ranges. **2** showed 24.7% loss (calc. 8%) between 240–547 °C, leaving CuO as residue, while **4** underwent a gradual 87.65% loss (calc. 89.26%) up to 650 °C, yielding a residue of 9.13% (calc. 8.42%). The closer agreement of experimental and calculated values for **4** suggests a more complete decomposition relative to the Zn frameworks.

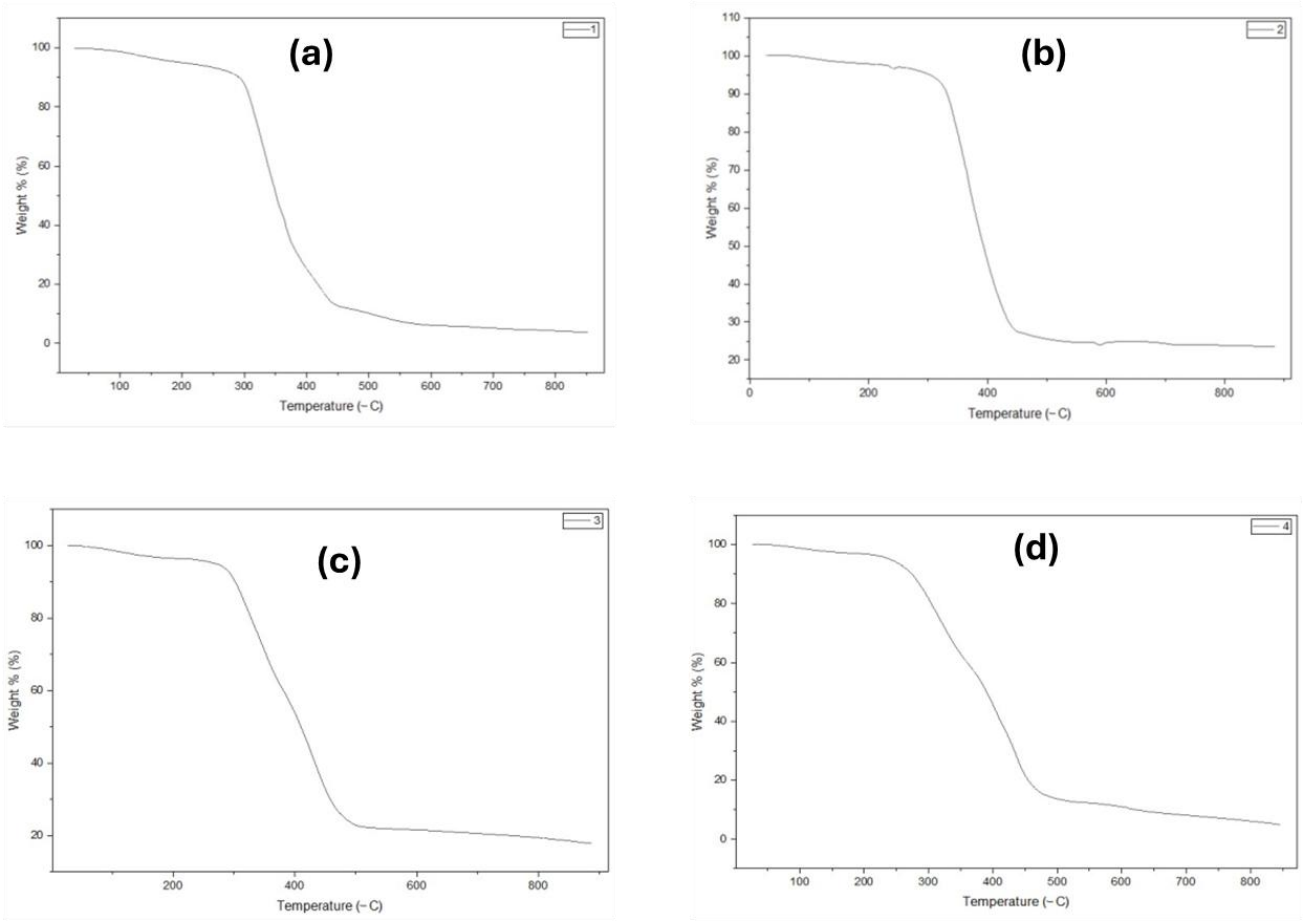

Figure 3. Thermogravimetric analysis (TGA) curves of the synthesized CPs: (a) $[Zn(BDC)_2(TMP)_2].2H_2O$ (**1**), (b) $[Cu(BDC)_2(TMP)_2].2H_2O$ (**2**), (c) $[Zn(PDC)_2(BTEC)_2]_n.2H_2O$ (**3**), and (d) $[Cu(PDC)_2(BTEC)_2]_n.2H_2O$ (**4**), recorded under nitrogen atmosphere.

BET analysis

All CPs (**1**–**4**), exhibited Type II isotherms with no significant hysteresis, consistent with monolayer–multilayer adsorption and limited microporosity [18]. The Zn-based frameworks showed lower BET surface areas (**1**: 163 m^2/g; **3**: 268 m^2/g) compared with the Cu-based

analogues (**2**: 291 m^2/g; **4**: 339 m^2/g). Micropore contributions followed the same trend, with **4** displaying the highest micropore surface area (411 m^2/g) and volume (0.302 cm^3/g) with a micropore diameter of 5.55 nm while **1**(micropore surface area: 187.07 m^2/g, micropore volume: 0.148 cm^3/g and micropore diameter: 2.70 nm), **2** (micropore surface area: 334.19 m^2/g, micropore volume: 0.266 cm^3/g and micropore diameter: 2.85 nm) and **3** (micropore surface area: 312.95 m^2/g, micropore volume: 0.240 cm^3/g and micropore diameter: 2.78 nm) have lower porosities.

These results demonstrate that Cu-based frameworks provide enhanced porosity over their Zn analogues, likely due to reduced interpenetration and more accessible pore networks (Figure 4).

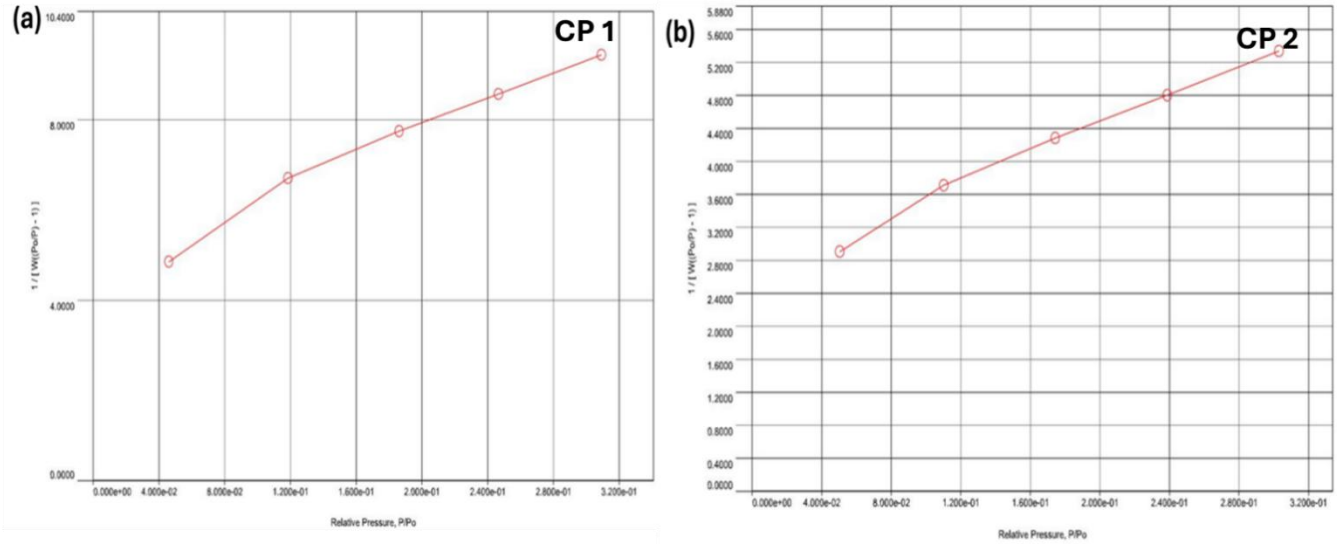

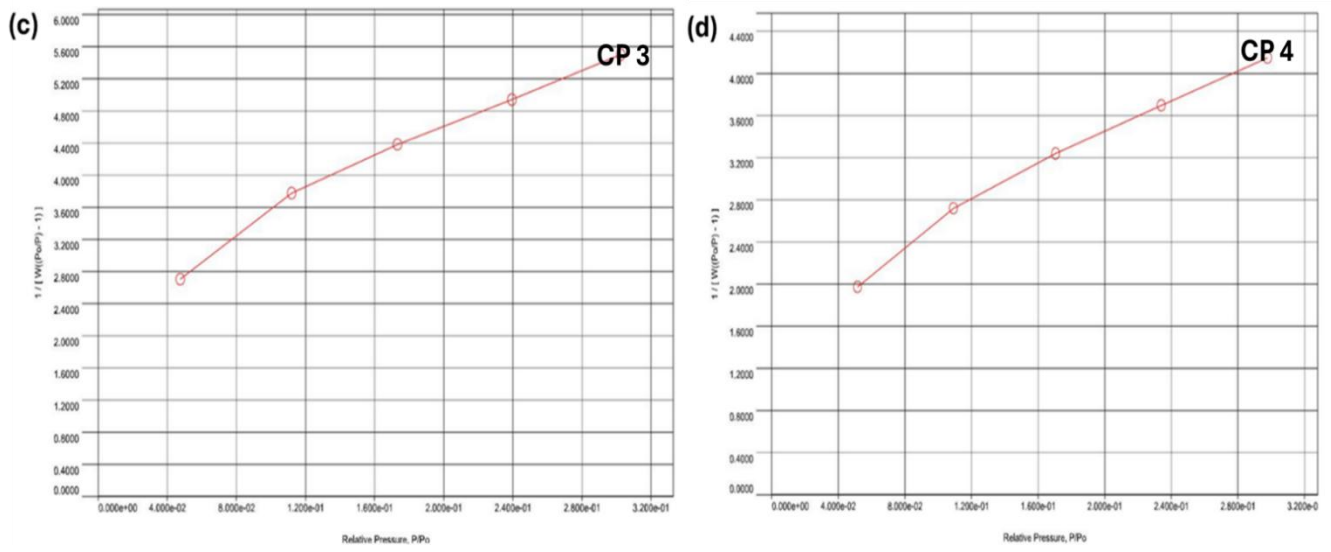

Figure 4: Multipoint BET plots for (a) CP 1 (b) CP 2 (c) CP 3 and (d) CP 4

Scanning Electron Microscopy

The SEM images of sample **1** (Figure 4a and 4b) show a highly agglomerated microstructure composed of irregularly shaped, clustered particles with flaky and layered surfaces, while **2** shows agglomerated irregularly shaped clusters which appear loosely packed with rough surfaces (Figure 4c and 4d). These aggregated features of samples **1** and **2** are associated with partial crystallinity and interparticle voids, which may contribute to their microporosities.

Sample **3** shows a compact, layered, and slab-like structure, with dense surfaces and minimal visible porosity (Figure 4e and 4f). This morphology differs from the porous appearance of **2** and the flaky clusters of **1**, reflecting the influence of polycarboxylate linkers where crystal stacking can obscure accessible pores.

In comparison, sample **4** appears more uniform, with polyhedron particles having well-defined edges (Figure 4g and 4h). The particles display moderate intergrowth, forming compact agglomerates with interconnected voids.

This improved particle regularity is consistent with the higher micropore contribution observed in the BET analysis and is distinct from the irregular clustering of samples **1** and **2** as well as the dense stacking of sample **3**.

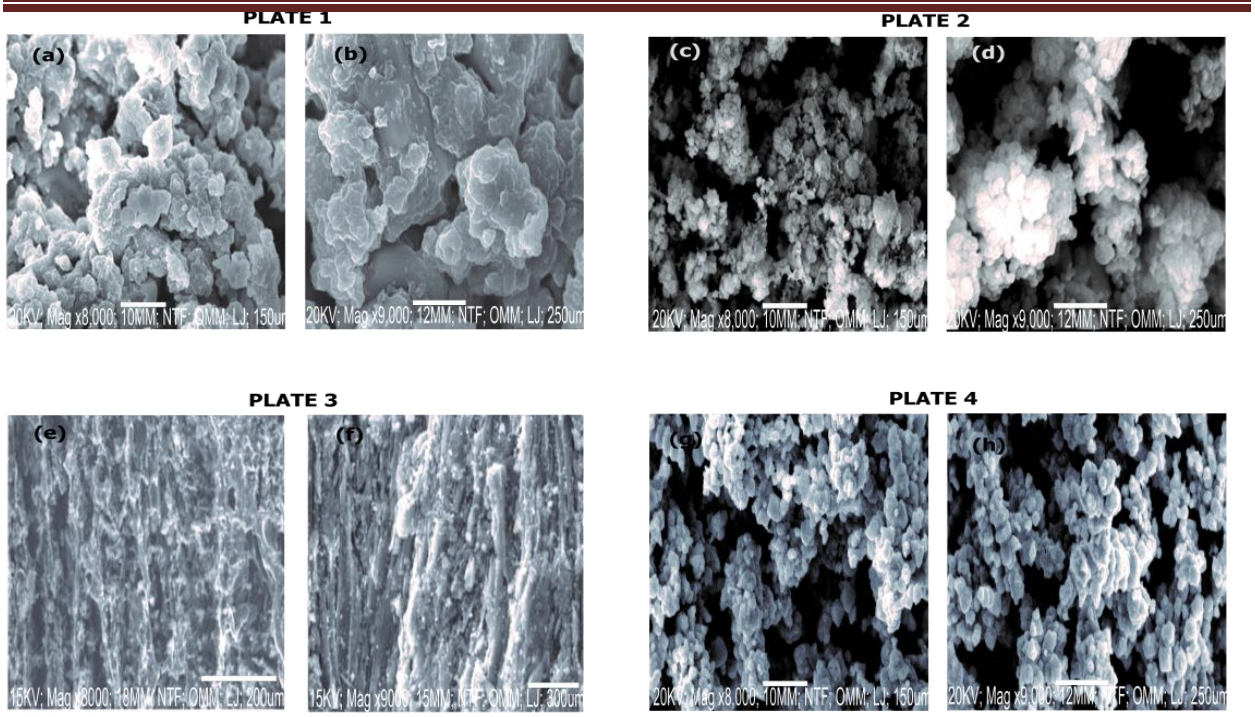

Figure 4. SEM micrographs of the synthesized CPs: Plate 1 (a, b) $[Zn(BDC)_2(TMP)_2]_n.2H_2O$ **1**, Plate 2 (c, d) $[Cu(BDC)_2(TMP)_2]_n.2H_2O$ **2**, Plate 3 (e, f) $[Zn(PDC)_2(BTEC)_2]_n.2H_2O$ **3**, and Plate 4 (g, h) $[Cu(PDC)_2(BTEC)_2]_n.2H_2O$ **4**. Each compound is shown at two magnifications (×8000 and ×9000), highlighting differences in particle morphology, crystallinity, and surface texture.

Photoluminescence Spectroscopy

The solid-state photoluminescence properties of the ligands and the corresponding CPs were investigated in the solid-state and at room temperature (Figure 5).

For Compound **1**, the excitation spectrum of 1,4-benzenedicarboxylic acid (BDC) monitored at 581 nm displayed a sharp band at 290 nm, while 4,4-trimethylenedipyridine (TMP) exhibited a weak peak at 390 nm when monitored at 535 nm. The emission spectrum of BDC showed a strong band at 581 nm (λex = 290 nm), and TMP displayed an emission maximum at 535 nm (λex = 270 nm). These bands are attributed to $\pi \rightarrow \pi^*$ and $n \rightarrow \pi^*$ transitions within the ligands [16]. In contrast, the spectrum of complex (**1**) exhibited an intense emission band at 515 nm upon excitation at 373 nm (Figure 5a). The similarity of this emission to TMP suggests that the luminescence of **1** originates mainly from the TMP ligand, while the observed blue shift relative to the free ligands is attributed to metal–ligand coordination effects.

In Compound **2**, the emission spectra of the free ligands were similar to those described above. The complex displayed an emission band at 521 nm when excited at 380 nm (Figure 5b). This band is assigned to ligand-centred $\pi \rightarrow \pi^*$ and $n \rightarrow \pi^*$ transitions, confirming that the luminescence mainly arises from the ligands. The slight blue shift compared with the free ligands can be ascribed to the coordination of Cu(II) ions within the framework.

The free ligands of compounds **3** and **4** (PDC and BTEC) exhibited characteristic emissions at 571 nm (λex = 385 nm, PDC) and 581 nm (λex = 290 nm, BTEC), assigned to intra-ligand $\pi \rightarrow \pi^*$ and $n \rightarrow \pi^*$ transitions [19]. The CP complex, **3**, however, showed a strong emission at 495 nm upon excitation at 335 nm (Figure 5c). The ~80 nm blue shift compared with the ligands is attributed to the coordination of Zn(II) ions, which alters the electronic environment [20].

Similarly, for compound **4**, the ligands PDC and BTEC exhibited emission maxima at 571 nm (λex = 385 nm) and 581 nm (λex = 290 nm), respectively, again corresponding to $\pi \rightarrow \pi^*$ and $n \rightarrow \pi^*$ transitions. The Cu–MOF (**4**) displayed a broad emission band at 521 nm upon excitation at 380 nm (Figure 5d). This emission, originating from ligand-centred transitions, is slightly blue shifted (~60 nm) compared with the free ligands, attributable to coordination with Cu(II) ions.

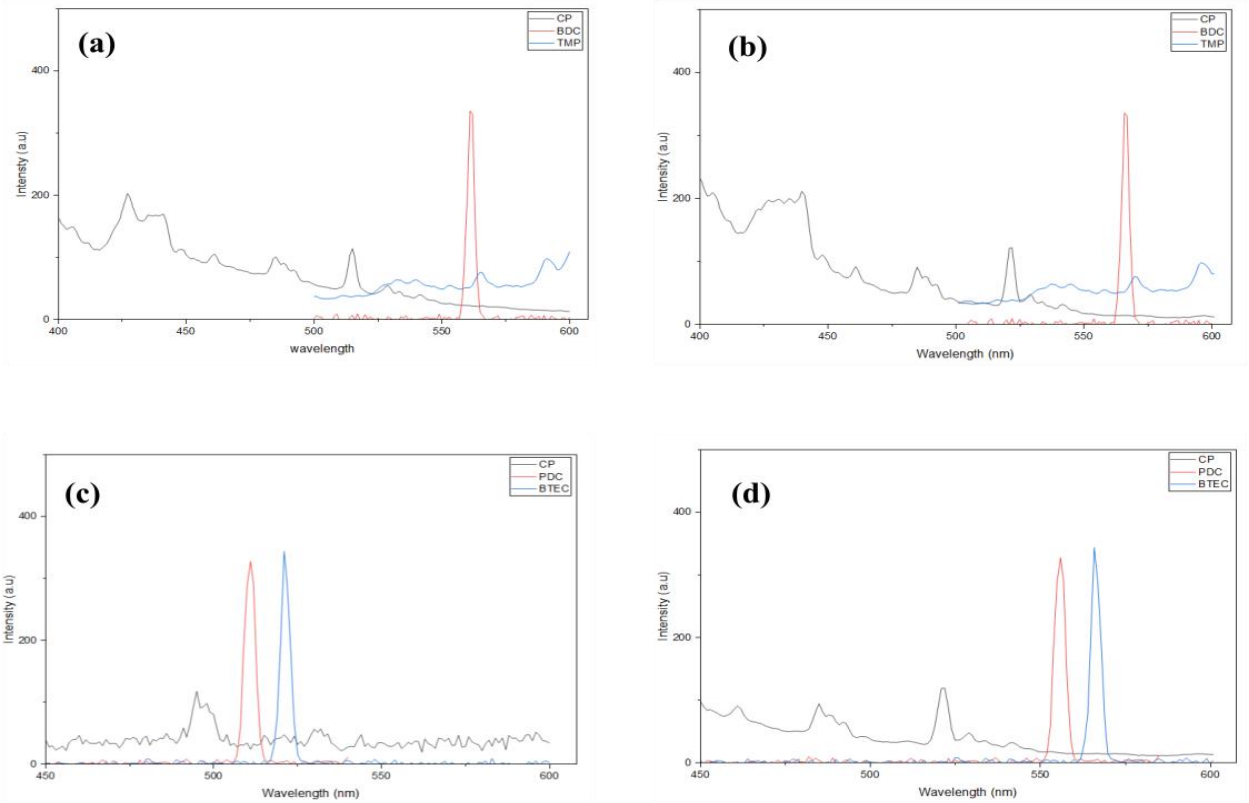

Figure 5. Photoluminescence spectra of ligands and CPs: (a) $[Zn(BDC)_2(TMP)_2]_n.2H_2O$ (**1**), (b) $[Cu(BDC)_2(TMP)_2]_n.2H_2O$ (**2**), (c) $[Zn(PDC)_2(BTEC)_2]_n.2H_2O$ (**3**), and (d) $[Cu(PDC)_2(BTEC)_2]_n.2H_2O$ (**4**)

CONCLUSION

Transition metal coordination polymers (4) based on Zn(II) and Cu(II) were successfully synthesized using mixed carboxylate and nitrogen donor ligands. FTIR confirmed coordination of the ligands to the metal centres, while UV/Vis spectra demonstrated characteristic π→π*, n→π*, LMCT, and d–d transitions. Photoluminescence analysis revealed blue-shifted emissions relative to the free ligands, confirming that the luminescence originates primarily from ligand-centred transitions modulated by metal–ligand coordination. The optical properties of these frameworks highlight their potential for applications in chemical sensing, luminescent probes, and optoelectronic devices. Future studies should investigate their performance in practical sensing applications, particularly in detecting environmental pollutants such as pesticides and heavy metals.

REFERENCES

1. Dey, C., Kundu, T., Biswal, B. P., Mallick, A., & Banerjee, R. (2013). Crystalline metal-organic frameworks (MOFs): synthesis, structure and function. *Acta Crystallographica Section B Structural Science, Crystal Engineering and Materials*, *70*(1), 3–10. https://doi.org/10.1107/s2052520613029557
2. Chiñas-Rojas, L. E., Vivar-Vera, G., Cruz-Martínez, Y. F., Colohua, S. L., Rivera, J. M., & Houbron, E. (2022). Transition Metals-Based Metal-Organic Frameworks, Synthesis, and Environmental Applications. *IntechOpen EBooks*. https://doi.org/10.5772/intechopen.104294
3. Espallargas, G. M., & Coronado, E. (2018). Magnetic functionalities in MOFs: from the framework to the pore. *Chemical Society Reviews*, *47*(2), 533–557. https://doi.org/10.1039/C7CS00653E
4. Wen, M., Li, G., Liu, H., Chen, J., An, T., & Yamashita, H. (2019). Metal–organic framework-based nanomaterials for adsorption and photocatalytic degradation of gaseous pollutants: recent progress and challenges. *Environmental Science: Nano*, *6*(4), 1006–1025. https://doi.org/10.1039/C8EN01167B
5. Jiang, C., Wang, L., Ouyang, Y., Lu, K., Jiang, W., Xu, H., … Sun, D. (2022). *Recent advances in metal–organic frameworks for gas adsorption/separation*. *4*(9), 2077–2089. https://doi.org/10.1039/d2na00061j
6. Hidetsugu Shiozawa, Bayer, B. C., Herwig Peterlik, Meyer, J. C., Lang, W., & Pichler, T. (2016). Doping of metal-organic frameworks towards resistive sensing. *ArXiv (Cornell University)*. https://doi.org/10.48550/arxiv.1611.09138
7. Bavykina, A., Kolobov, N., Khan, I. S., Bau, J. A., Ramirez, A., & Gascon, J. (2020). Metal–Organic Frameworks in Heterogeneous Catalysis: Recent Progress, New Trends, and Future Perspectives. *Chemical Reviews*, *120*(16), 8468–8535. https://doi.org/10.1021/acs.chemrev.9b00685.
8. Hussain, S., Chen, X., Gao, Y., Song, H., Tian, X., He, Y., … Gao, R. (2023). Unveiling the Transformation from Aggregation-Caused Quenching to Encapsulation-Induced Emission Enhancement for Improving the Photoluminescence Properties and Detection Performance of Conjugated Polymer Material in Multiple States. *Advanced Optical Materials*, *11*(12). https://doi.org/10.1002/adom.202202851
9. Cui, Y., Yue, Y., Qian, G., & Chen, B. (2011). Luminescent Functional Metal–Organic Frameworks. *Chemical Reviews*, *112*(2), 1126–1162. https://doi.org/10.1021/cr200101d

10. Guo, B.-B., Yin, J.-C., Li, N., Fu, Z.-X., Han, X., Xu, J., & Bu, X.-H. (2021). Recent Progress in Luminous Particle-Encapsulated Host–Guest Metal-Organic Frameworks for Optical Applications. *Advanced Optical Materials*, *9*(23). https://doi.org/10.1002/adom.202100283
11. Stock, N., & Biswas, S. (2011). Synthesis of Metal-Organic Frameworks (MOFs): Routes to Various MOF Topologies, Morphologies, and Composites. *Chemical Reviews*, *112*(2), 933–969. https://doi.org/10.1021/cr200304e
12. Nakamoto, K. (2009). *Infrared and Raman Spectra of Inorganic and Coordination Compounds : Applications in Coordination, Organometallic, and Bioinorganic Chemistry*. John Wiley & Sons.
13. Pavia, D. L., Lampman, G. M., Kriz, G. S., & Vyvyan, J. A. (2014). *Introduction to Spectroscopy*. Cengage Learning.
14. Grasseschi, D., & Toma, H. E. (2017). The SERS effect in coordination chemistry. *Coordination Chemistry Reviews*, *333*, 108–131. https://doi.org/10.1016/j.ccr.2016.11.019
15. Nazari, Z., Taher, M. A., & Fazelirad, H. (2017). A Zn based metal organic framework nanocomposite: synthesis, characterization and application for preconcentration of cadmium prior to its determination by FAAS. *RSC Advances*, *7*(71), 44890–44895. https://doi.org/10.1039/c7ra08354h
16. Shin, C., Kim, J., & Huh, S. (2023). Fluorescent and Catalytic Properties of a 2D Lamellar Zn Metal–Organic Framework with sql Network Structure. *Molecules*, *28*(17), 6357–6357. https://doi.org/10.3390/molecules28176357
17. Wang, C.-C., Ke, S.-Y., Cheng, C.-W., Wang, Y.-W., Chiu, H.-S., Ko, Y.-C., … Lee, G.-H. (2017). Four Mixed-Ligand Zn(II) Three-Dimensional Metal-Organic Frameworks: Synthesis, Structural Diversity, and Photoluminescent Property. *Polymers*, *9*(12), 644–644. https://doi.org/10.3390/polym9120644
18. Françoise Rouquerol, J Rouquerol, K. S. W Sing, Llewellyn, P. L., & G Maurin. (2014). *Adsorption by powders and porous solids: principles, methodology and applications*. Elsevier/Ap.
19. Jornet-Mollá, V., Martín-Mezquita, C., Giménez-Saiz, C., & Romero, F. M. (2022). Zinc(II) picolinate-based coordination polymers as luminescent sensors of Fe3+ ions and nitroaromatic compounds. *Inorganica Chimica Acta*, *538*, 120993. https://doi.org/10.1016/j.ica.2022.120993
20. Kuznetsova, A., Matveevskaya, V., Pavlov, D., Yakunenkov, A., & Potapov, A. (2020). Coordination Polymers Based on Highly Emissive Ligands: Synthesis and Functional Properties. *Materials*, *13*(12), 2699. https://doi.org/10.3390/ma13122699